

FULL PAPER

# Structural relaxation behavior of nano silicon-graphite composite anode after lithium-ion insertion

Jiawei Fu<sup>1</sup>, Takeshi Yabutsuka<sup>1</sup> and Shigeomi Takai<sup>1,†</sup>

<sup>1</sup>Graduate School of Energy Science, Kyoto University, Yoshida-Honmachi, Sakyo-ku, Kyoto 606-8501, Japan

The relaxation behavior of nano silicon-graphite composite anode in lithium-ion half-cell just after the termination of lithiation has been investigated by the X-ray diffraction (XRD) method under argon atmosphere. The diffraction peaks of stage I of lithium graphite intercalation compound (Li-GIC) turned into those of stage II during the relaxation process, indicating that lithium-ions migrated from Li-GIC into Si toward the equilibrium lithium distribution between Li-GIC and Si side. While the amounts of lithium-ion migration were related to the amount of Si content in the anode, the rate constant depends on the charging current density.

Key-words : Structural relaxation, Lithium-ion battery, Silicon-graphite composite anode, X-ray diffraction, Lithium migration

[Received October 10, 2024; Accepted December 11, 2024; Published online January 15, 2025]

## 1. Introduction

As the most commonly used anode material for lithium-ion batteries,<sup>1)</sup> graphite has the advantages of a sufficiently flat and low voltage profile and low cost.<sup>2-4)</sup> Graphite has a well-defined stage structure as the lithium-ion intercalated into the graphene layers. A stage  $n$  can be defined as the number of consecutive graphene layers between intercalate layers.<sup>1)</sup> The stage II is formed when lithium-ions occupy every two graphene layers with the formula of  $\text{LiC}_{12}$ , and the fully lithiated  $\text{LiC}_6$ , known as stage I, has a structure with lithium-ion between every graphene layer. On the other hand, a theoretical capacity of  $372 \text{ mA}\cdot\text{h}\cdot\text{g}^{-1}$  is no longer sufficient for the demands of electric vehicle and energy storage systems.<sup>1,5)</sup> Silicon, with its high theoretical capacity ( $3580 \text{ mA}\cdot\text{h}\cdot\text{g}^{-1}$  as  $\text{Li}_{15}\text{Si}_4$  at room temperature,  $4200 \text{ mA}\cdot\text{h}\cdot\text{g}^{-1}$  as  $\text{Li}_{21}\text{Si}_5$  at  $415^\circ\text{C}$ )<sup>6,7)</sup> and abundant reserves on Earth,<sup>8)</sup> is considered the next-generation anode material for lithium-ion secondary batteries. However, because of the disadvantages of Si, such as significant volumetric change during charge and discharge cycles (up to  $\sim 300\%$ )<sup>9)</sup> and poor lithium-ion conductivity, it is commonly used by mixing with graphite to form a composite anode.<sup>10-12)</sup> This combination introduces the challenge of understanding the interaction between the two materials.<sup>13,14)</sup>

During charging, the Si is firstly lithiated,<sup>15,16)</sup> whereas the lithiation of graphite starts at a relatively lower potential,<sup>17)</sup> and finally the stage I is formed at a potential of lower than  $70 \text{ mV}$ .<sup>18,19)</sup> At the termination of lithiation, the lithium distributions in Si and graphite are thought to be

different from the equilibrium ones.<sup>20)</sup> Then the relaxation analysis using X-ray diffraction coupled with the structure analysis is adopted to the Si-graphite system. Although lithium redistribution in Si-graphite composite anodes has been previously reported, these studies were either conducted at relatively early stages of charging,<sup>6)</sup> low temperatures,<sup>21)</sup> or in-situ XRD,<sup>22)</sup> making it difficult to directly obtain information on the relaxation behavior of the system.

The structural relaxation phenomena of various cathode and anode materials have been investigated after the lithium insertion or extraction,<sup>23-32)</sup> showing the transition from kinetically favorable states toward equilibrium. These results provide important insights for understanding the properties of battery materials. In our previous study, we investigated the structural relaxation behavior of silicon monoxide (SiO) graphite composite after lithium intercalation, and a re-distribution occurred between the Li-GIC and SiO, due to lithium-ion consumption from irreversible reactions,<sup>31)</sup> and the migrated amount is related to the content of SiO.<sup>33)</sup> However, this lithium-ion migration decreases after several charging-discharging cycles which were attributed by the degradation of SiO.<sup>32)</sup> However, to further increase the anode capacity, it is necessary to study the Si and graphite composite anode instead of SiO, therefore, studying the relaxation behavior between Si and graphite in the composite anode is significant.

Here, we focused on the stage transitions exhibited by Li-GIC in Si-graphite composite anodes, since the amorphous nature of lithium silicide (Li-Si) intermetallic compound does not show distinct XRD peaks.<sup>34,35)</sup> The relaxation analysis based on the stage variation of Li-GIC provides insights into the redistribution of lithium-ions between graphite and Si.

<sup>†</sup> Corresponding author: S. Takai; E-mail: [stakai@energy.kyoto-u.ac.jp](mailto:stakai@energy.kyoto-u.ac.jp)

In this study, we applied relaxation analysis to the Si-graphite composite anode to investigate lithium migration within the anode. The migrated amount and rate constant were then analyzed and discussed.

## 2. Experimental

Working electrode compound was prepared by mixing the slurry of nano-size silicon (<100 nm, Fuji Film Wako, Japan), natural graphite (LB-GC, Nippon Graphite, Japan), Acetylene black (A. B.) and polyvinylidene difluoride (PVdF) with the weight ratios of 10:80:3:7, 15:75:3:7, and 30:60:3:7, which are denoted as 10-Si, 15-Si and 30-Si, respectively. The compound was then spread on a copper foil with a small amount of *N*-Methyl-2-pyrrolidone solvent followed by drying in an incubator maintained at 60 °C. Two-electrode test cells (Hohsen, Japan) were assembled using lithium metal as counter electrode and a solution of 1 M LiPF<sub>6</sub> with ethylene carbonate (EC)/dimethyl carbonate (DMC) (2:1 v/v, Kishida Chem., Japan) was used as the electrolyte. The theoretical capacities were evaluated based on the weighted sum for the Si and graphite, which corresponded to 3580 mA·h·g<sup>-1</sup> to form Li<sub>15</sub>Si<sub>4</sub><sup>6,34</sup> and 372 mA·h·g<sup>-1</sup> for LiC<sub>6</sub>,<sup>19</sup> respectively. The sample compositions and estimated theoretical capacities are listed in **Table 1**. Electrochemical lithium intercalation was carried out using a galvanostat (HJ-SD8, Hokuto Denko, Japan) with current densities of 0.04C-rate and 0.1C-rate for 25 and 10 h of charging, respectively.

After the working electrodes were lithiated to the theoretical capacities, we removed the electrodes from the cell, washed with EC and EC/DMC solvents and subsequently dried,<sup>36</sup> then mounted on a sealed holder with beryllium window (2391A201, Rigaku Corp., Japan) inside an argon-gas filled glove box. The sealed holder was placed in an X-ray diffractometer (Ultima IV, Rigaku Corp., Japan) with Cu K $\alpha$  radiation (40 kV and 40 mA). At a scanning rate of 5° per minute, X-ray diffraction measurements were performed over a 2 $\theta$  range of 11 to 53° with a step size of 0.01°. These diffraction experiments were repeated at designated relaxation intervals for up to 24 h.

The obtained XRD profiles were analyzed by the one-dimensional version of the Rietveld analysis code, RIEVEC.<sup>37–39</sup> The mole fraction of the stage I was calculated as<sup>40</sup>

$$M_I = S_I Z_I V_I / (S_I Z_I V_I + S_{II} Z_{II} V_{II}) \quad (1)$$

where  $M_I$  is the mole fraction of stage I, and  $S$ ,  $Z$ , and  $V$  are the scale factor, number of chemical formulae in a unit

**Table 1.** Weight ratio of Si and graphite in the composites and the corresponding capacities

Sample	Si % w/w	graphite % w/w	A. B. % w/w	PVdF % w/w	Capacity (mA·h·g <sup>-1</sup> )
10-Si	10	80	3	7	728
15-Si	15	75	3	7	906
30-Si	30	60	3	7	1441
45-Si	45	45	3	7	1976

cell, and volume of unit cell for each stage. Subscripts I and II denote the stages I and II, respectively.

## 3. Results and discussion

The charging curves for composite anodes with various Si contents are represented in **Fig. 1**. As seen from these curves, the lithium-ions were first inserted into Si at above 0.2 V,<sup>15</sup> while the lithiation of graphite started at lower potential. The potential eventually decreased to that of stage I of Li-GIC at the end of charging,<sup>41,42</sup> indicating that lithium-ions were inserted into graphite as well as Si. The Si side might be lithium deficient due to solid electrolyte interphase (SEI) formation under large volumetric change,<sup>34</sup> and lithium migration from the fully lithiated Li-GIC may provide lithium-ion to Si. However, it is noteworthy that as the Si content increased to 45-Si, lithium plating occurred as the negative potential plateau in Fig. 1, and no further changes in the XRD profile were observed during the relaxation. **Figure 2** shows the XRD profile of Si-graphite composite anode with Si contents ranging from 10-Si to 30-Si after 0.04C-rate and 0.1C-rate lithiation. The diffraction peaks of stage I are detected for all the samples just after lithiation (0 h of relaxation), whereas the peaks of stage II gradually increase during relaxation. Here, the diffraction peaks of the Li-Si compound were not detected due to its amorphous structure.<sup>43</sup>

Rietveld analysis was conducted to obtain the detailed stage transitions of Li-GIC during the relaxation period. **Figure 3** presents a representative refined profile of 15-Si charged at a 0.1C-rate after 3 h of relaxation. The sufficiently small  $R_{wp}$  value indicates that the diffraction profile matches well with the measured data, assuming the coexistence of stage I and stage II. The lattice parameters obtained from the Rietveld analysis and the calculated mole fractions of stage I are shown in **Figs. 4** and **5**. Additionally, the mole fraction of stage I in Si-graphite composite anodes with different Si contents, compared to that of a pure graphite anode, is shown in **Fig. 6**.

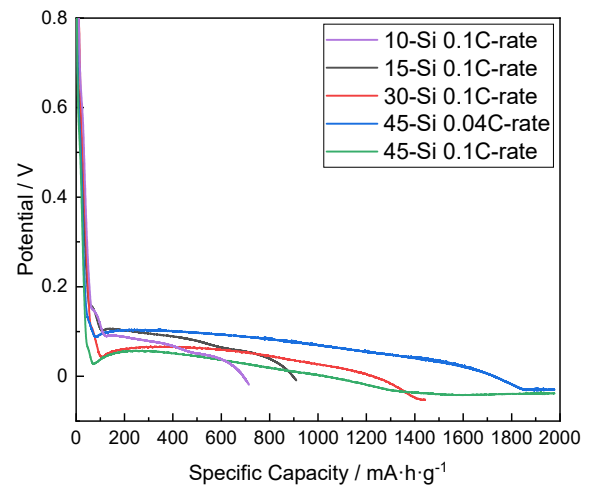


**Fig. 1.** Comparison of charging curves from 10-Si, 15-Si, 30-Si and 45-Si. Lithium plating happened while Si content reached to 45-Si for both 0.04C-rate and 0.1C-rate.

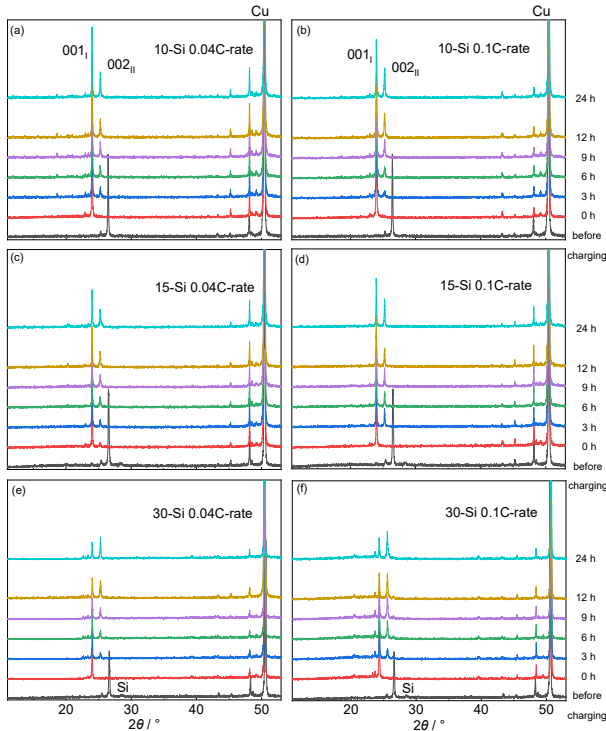


**Fig. 2.** X-ray diffraction profiles of Si-graphite anode for (a), (b) 10-Si, (c), (d) 15-Si, and (e), (f) 30-Si. The rates for lithiation are (a), (c), (e) for 0.04C-rate, and (b), (d), (f) for 0.1C-rate. Relaxation times after charging are indicated at the right side of the profiles, and those before charging are also shown as reference. Diffraction peaks of current collector copper are shown. Some extra small peaks are attributed to the copper foil. The peak of Si is only detected for the pattern before charging.

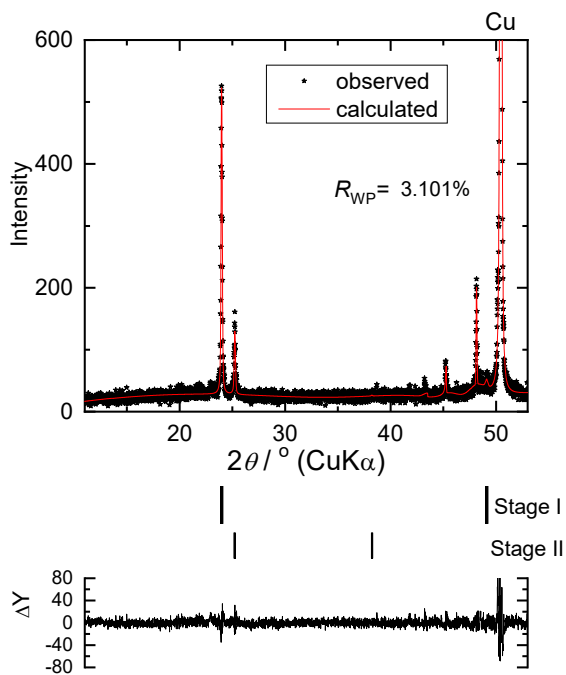


**Fig. 3.** Example of the Rietveld analysis of the 15-Si 0.1C-rate sample after 3 h of relaxation.

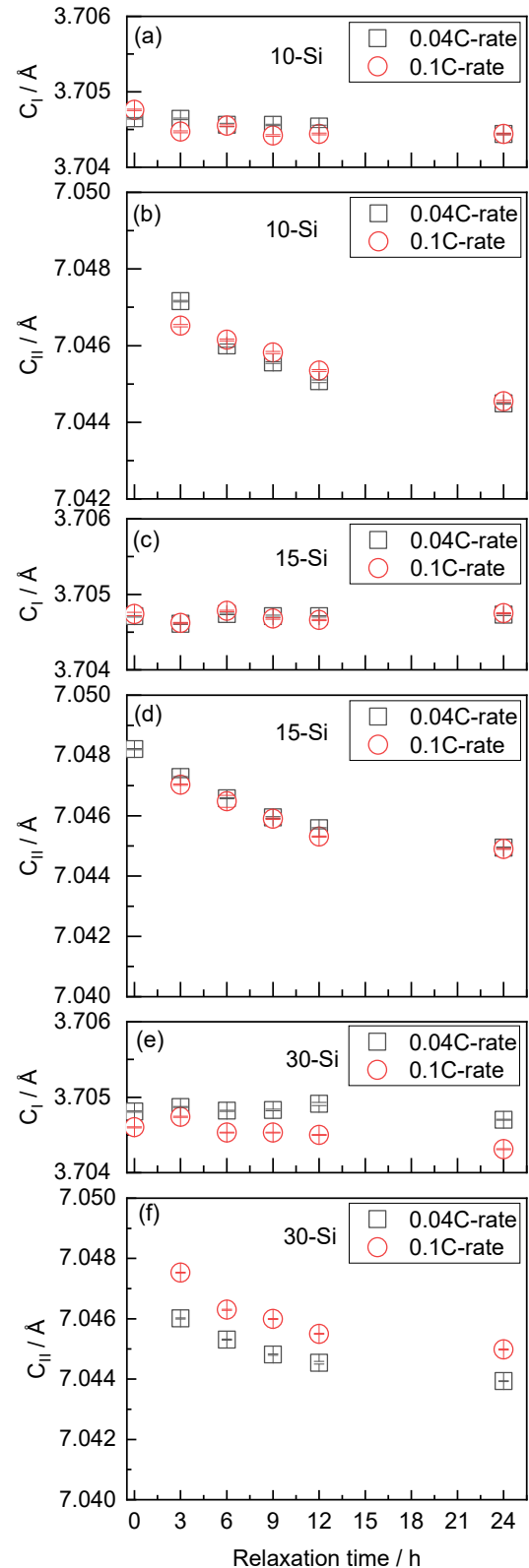


**Fig. 4.** Refined lattice parameters  $c$  for (a) stage I and (b) stage II of 10-Si, (c) stage I and (d) stage II of 15-Si and (e) stage I and (f) stage II of 30-Si anode plotted versus relaxation time. The current densities for lithiation are black square for 0.04C-rate, and red circle for 0.1C-rate.

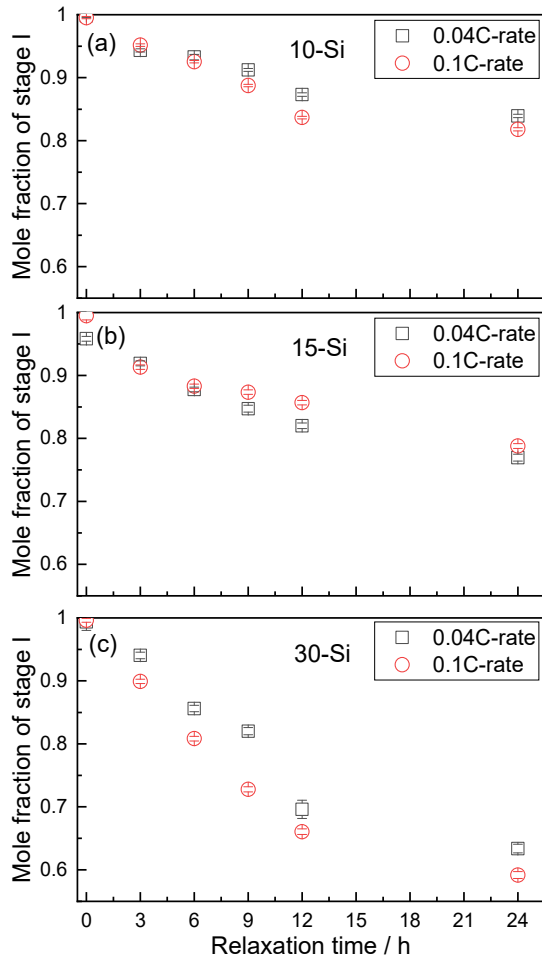


**Fig. 5.** Calculated mole fraction of stage I for Li-GIC of (a) 10-Si, (b) 15-Si and (c) 30-Si anode plotted versus relaxation time. The current densities for lithiation are black square for 0.04C-rate, and red circle for 0.1C-rate.

The relaxation time dependence for  $c$ -axis length of stage I and II is shown in Fig. 4. For stage I of Li-GIC, the  $c$ -axis length is insensitive to the lithium concentration,<sup>18,44,45</sup> remaining approximately constant at  $c_1 \approx 3.704 \text{ \AA}$  during relaxation. In contrast,  $c_{II}$  decreases from 7.049 to 7.044  $\text{\AA}$ , which is consistent with the in-situ experiments.<sup>18,45</sup>

In Figs. 5 and 6, it can be observed that the mole fraction of stage I after 24h of relaxation reduces with an increasing weight ratio of Si, indicating that this change is not only due to defect ordering<sup>23</sup>) within Li-GIC but also the lithium migration from Li-GIC into Si. In addition, the mole fraction of stage I varies with charging current density during the first 12 h of relaxation, whereas the mole fraction at the relaxed data (24 h) shows little difference. This dependency on the charging rate is especially pronounced with increasing Si content in samples. Furthermore, for composite anodes with higher Si content above 15-Si, Fig. 6 shows a larger reduction in the mole fraction of stage I compared to the pure graphite anode, which further supports the lithium migration from Li-GIC to Si. The reduction in the equilibrium mole fraction of stage I with increased Si content might be due to larger amount of

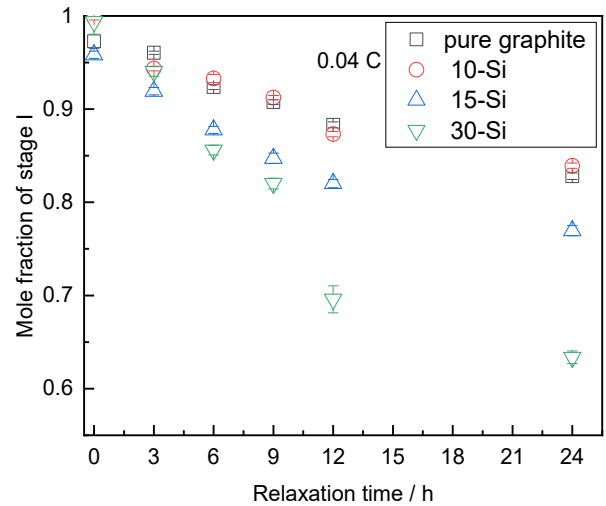


**Fig. 6.** Comparison of mole fraction of stage I between pure graphite anode and Si-graphite composite anodes with a relaxation of 24 h.

lithium-ion consumption associated with increased surface area of the nano-size Si.<sup>46,47</sup>) On the other hand, the 30-Si composite anode exhibits smaller transition on mole fraction of stage I than that of SiO-graphite composite anode denoted as 30-SiO (SiO:graphite:A.B.:PVdF = 30:60:3:7 in weight ratios) from our previous work,<sup>31</sup>) indicating less lithium migration during relaxation. This difference may be due to the greater irreversible lithium loss from the reaction of lithium-ions with SiO compared to Si during the first lithiation,<sup>13,48</sup>) thus a more severe lithium deficiency after termination of lithiation and a greater lithium loss from Li-GIC were observed in comparison with the Si composite anode.

**Figure 7** illustrates the dependence of Li content in Li-GIC on relaxation time based on the refined mole fraction of stage I. Here, stage I and II of Li-GIC are assumed to correspond to  $\text{LiC}_6$  and  $\text{LiC}_{12}$ , respectively. As relaxation process proceeds, the value of  $x$  in  $\text{Li}_x\text{C}_6$  gradually decreases, and  $x$  reaches a certain value after 24 h of relaxation, which appears to be close for both 0.04C and 0.1C-rate samples with the same Si content. On the other hand, the 0.1C-rate sample exhibits slightly faster decrease comparing with the 0.04C-rate. Assuming that the lithium migration rate from Li-GIC is proportional to the difference between the equilibrium Li content,<sup>31</sup>) the lithium concentration can be expressed by the following formulae of the primary reaction.

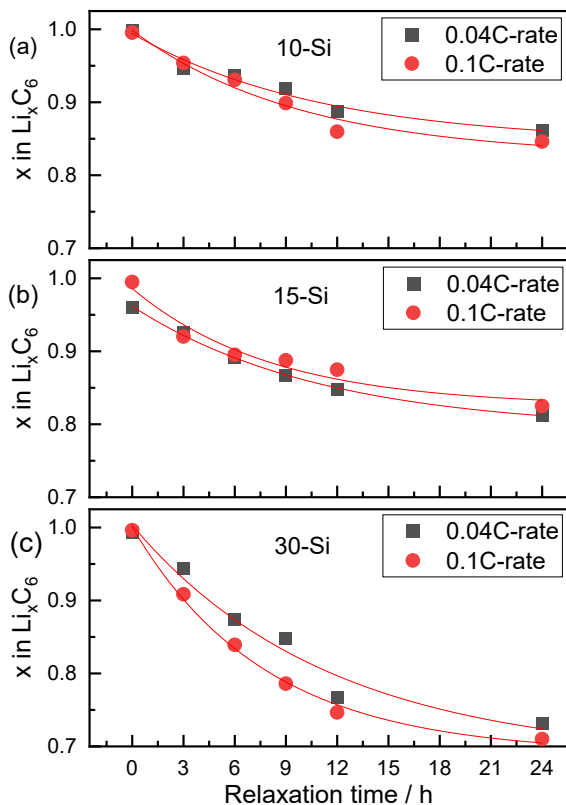
$$x = (x_0 - x_{\text{eq}})e^{-\alpha t} + x_{\text{eq}} \quad (2)$$

Here,  $\alpha$  represents the rate constant of the primary reaction,  $x_{\text{eq}}$  denotes the lithium concentration at equilibrium, and  $x_0 - x_{\text{eq}}$  represents the change in lithium concentration during relaxation. The fitted relaxation curves are also shown in Fig. 7, demonstrating a good match with the measured data. The parameters obtained through the fitting process are listed in **Table 2**.

From Fig. 7 and Table 2, it appears that  $x_{\text{eq}}$  decreases an increasing amount of Si in the composite, which is little

**Table 2.** Fitted parameters of relaxation curve of the lithium content in the  $\text{Li}_x\text{C}_6$  in composite anode

Sample	10-Si		15-Si		30-Si	
	0.04C-rate	0.1C-rate	0.04C-rate	0.1C-rate	0.04C-rate	0.1C-rate
$x_{\text{eq}}$	0.844(22)	0.825(23)	0.792(5)	0.824(22)	0.684(51)	0.690(12)
$x_0 - x_{\text{eq}}$	0.150(21)	0.173(22)	0.170(5)	0.161(23)	0.319(48)	0.310(13)
$\alpha$	0.091(30)	0.101(31)	0.090(6)	0.122(43)	0.087(30)	0.128(13)
$R^2$	0.971	0.971	0.99	0.95	0.97	0.99

**Fig. 7.** Calculated relaxation-time dependence of lithium content in Li-GIC and the fitting curves.

dependency to the charging current density. The lithiation of Si does not reach its theoretical capacity because some of the lithium-ions are consumed by the formation of SEI. It is reasonable to conclude that the deficiency of lithium-ions in Si increases with Si content, resulting in a decrease in  $x_{\text{eq}}$  on the Li-GIC side. The rate constant is not so varied at 0.04C-rate, although the rate constant increases with the increase in Si content for the sample at 0.1C-rate, which is more pronounced between 10-Si and 15-Si. This behavior differs from that observed in SiO-graphite composite anodes, where the rate constants at both 0.04C-rate and 0.1C-rate are independent of SiO content.<sup>31)</sup> This may be attributed to the lower lithium-ion diffusion coefficient of Si compared to that of SiO,<sup>49)</sup> making the change in lithium-ion content more noticeable with varying Si content.

In this study, the relaxation behavior of Si-graphite composite anode was analyzed through XRD combined with the Rietveld analysis method. Our findings reveal that the

lithium-ions migrate from Li-GIC into Si during relaxation toward an equilibrium state. The Si content in the present investigation range seems to be irrelevant to the lithium migration rate under lower current density, whereas a higher current density contributes to a slightly faster migration with Si content. These findings would provide valuable insights for the research and development of high-energy density lithium-ion batteries.

#### 4. Conclusion

The relaxation behavior of fully lithiated nano Si-graphite composite anodes was analyzed through X-ray diffraction in combination with the one-dimensional Rietveld refinement method over a period of up to 24 h. A reduction in the mole fraction of stage I was observed across all samples, suggesting that lithium-ions were extracted from Li-GIC. While the  $c$ -axis of stage II shrinks during the relaxation period, that of stage I remains almost constant. The amount of migrated lithium-ions is well described by the primary reaction formulae, from which the deduced rate constants are significantly related to the charging current density rather than the Si content. These results not only clarify lithium migration during relaxation but also provide valuable insights for practical applications during the resting period after charging.

#### References

- 1) J. Asenbauer, T. Eisenmann, M. Kuenzel, A. Kazzazi, Z. Chen and D. Bresser, *Sustain. Energy Fuels* **4**, 5387 (2020).
- 2) H. Azuma, H. Imoto, S. N. I. Yamada and K. Sekai, *J. Power Sources* **81–82**, 1 (1999).
- 3) H. Zhang, Y. Yang, D. Ren, L. Wang and X. He, *Energy Storage Mater.* **36**, 147 (2021).
- 4) A. Missyul, I. Bolshakov and R. Shpanchenko, *Powder Diffr.* **32**, S56 (2017).
- 5) Y. Nishi, *J. Power Sources* **100**, 101 (2001).
- 6) C. Heubner, T. Liebmann, O. Lohrberg, S. Cangaz, S. Maletti and A. Michaelis, *Batter. Supercaps.* **5**, e20210018 (2022).
- 7) H. J. Lee, J. S. Moon, Y. W. Byeon, W. Y. Yoon, H. K. Kim and J. P. Ahn, *ACS Energy Lett.* **7**, 2469 (2022).
- 8) L. Sun, Y. Liu, J. Wu, R. Shao, R. Jiang, Z. Tie and Z. Jin, *Small* **18**, 1 (2022).
- 9) J. W. Wang, X. H. Liu, K. Zhao, A. Palmer, E. Patten, D. Burton, S. X. Mao, Z. Suo and J. Y. Huang, *ACS Nano* **6**, 9158 (2012).
- 10) S. B. Son, L. Cao, T. Yoon, A. Cresce, S. E. Hafner, J. Liu, M. Groner, K. Xu and C. Ban, *Adv. Sci.* **6**, 1 (2019).
- 11) X. Feng, J. Yang, Q. Lu, J. Wang and Y. Nuli, *Phys. Chem. Chem. Phys.* **15**, 14420 (2013).

- 12) K. P. C. Yao, J. S. Okasinski, K. Kalaga, J. D. Almer and D. P. Abraham, *Adv. Energy Mater.* **9**, 1 (2019).
- 13) W. Ai, N. Kirkaldy, Y. Jiang, G. Offer, H. Wang and B. Wu, *J. Power Sources* **527**, 231142 (2022).
- 14) D. P. Finegan, A. Vamvakeros, L. Cao, C. Tan, T. M. M. Heenan, S. R. Daemi, S. D. M. Jacques, A. M. Beale, M. Di Michiel, K. Smith, D. J. L. Brett, P. R. Shearing and C. Ban, *Nano Lett.* **19**, 3811 (2019).
- 15) S. Chae, S. H. Choi, N. Kim, J. Sung and J. Cho, *Angew. Chem. Int. Edit.* **59**, 110 (2020).
- 16) C. L. Berhaut, D. Z. Dominguez, P. Kumar, P. H. Jouneau, W. Porcher, D. Aradilla, S. Tardif, S. Pouget and S. Lyonnard, *ACS Nano* **13**, 11538 (2019).
- 17) N. Nitta and G. Yushin, *Part. Part. Syst. Char.* **31**, 317 (2014).
- 18) S. Schweidler, L. De Biasi, A. Schiele, P. Hartmann, T. Brezesinski and J. Janek, *J. Phys. Chem. C* **122**, 8829 (2018).
- 19) T. Ohzuku, Y. Iwakoshi and K. Sawai, *J. Electrochem. Soc.* **140**, 2490 (1993).
- 20) C. L. Berhaut, M. Mirolo, D. Z. Dominguez, I. Martens, S. Pouget, N. Herlin-Boime, M. Chandesris, S. Tardif, J. Drnec and S. Lyonnard, *Adv. Energy Mater.* **13**, 1 (2023).
- 21) K. Richter, T. Waldmann, N. Paul, N. Jobst, R. G. Scurtu, M. Hofmann, R. Gilles and M. Wohlfahrt-Mehrens, *ChemSusChem* **13**, 529 (2020).
- 22) J. Moon, H. C. Lee, H. Jung, S. Wakita, S. Cho, J. Yoon, J. Lee, A. Ueda, B. Choi, S. Lee, K. Ito, Y. Kubo, A. C. Lim, J. G. Seo, J. Yoo, S. Lee, Y. Ham, W. Baek, Y.-G. Ryu and I. T. Han, *Nat. Commun.* **12**, 2714 (2021).
- 23) T. Kitamura, S. Takai, T. Yabutsuka and T. Yao, *J. Phys. Chem. Solids* **142**, 109440 (2020).
- 24) S. Takai, T. Kitamura, T. Yabutsuka and T. Yao, *Electrochemistry* **88**, 434 (2020).
- 25) A. Tamura, S. Takai, T. Yabutsuka and T. Yao, *J. Electrochem. Soc.* **164**, A1514 (2017).
- 26) J. Kang, S. Takai, T. Yabutsuka and T. Yao, *J. Electrochem. Soc.* **168**, 010518 (2021).
- 27) S. Park, M. Oda and T. Yao, *Solid State Ionics* **203**, 29 (2011).
- 28) Y. Satou, S. Komine, S. Park and T. Yao, *Solid State Ionics* **262**, 35 (2014).
- 29) I. S. Seo, S. Park and T. Yao, *ECS Electrochem. Lett.* **2**, 2 (2013).
- 30) I. S. Seo, S. Nagashima, S. Takai and T. Yao, *ECS Electrochem. Lett.* **2**, 72 (2013).
- 31) J. Fu, S. Takai, T. Yabutsuka and T. Yao, *J. Electrochem. Soc.* **171**, 020557 (2024).
- 32) J. Fu, S. Takai, T. Yabutsuka and T. Yao, *J. Ceram. Soc. Jpn.* **132**, 563 (2024).
- 33) X. Gao, S. Li, J. Xue, D. Hu and J. Xu, *Adv. Energy Mater.* **13**, 2202584 (2023).
- 34) J. Li and J. R. Dahn, *J. Electrochem. Soc.* **154**, A156 (2007).
- 35) M. T. McDowell, S. W. Lee, W. D. Nix and Y. Cui, *Adv. Mater.* **25**, 4966 (2013).
- 36) B. S. Lee, S. H. Oh, Y. J. Choi, M. J. Yi, S. H. Kim, S. Y. Kim, Y. E. Sung, S. Y. Shin, Y. Lee and S. H. Yu, *Nat. Commun.* **14**, 1 (2023).
- 37) Y. Oka, T. Yao and N. Yamamoto, *J. Mater. Chem.* **3**, 1031 (1993).
- 38) Y. Oka, T. Yao and N. Yamamoto, *J. Mater. Chem.* **3**, 1037 (1993).
- 39) T. Yao, N. Ozawa, T. Aikawa and S. Yoshinaga, *Solid State Ionics* **175**, 199 (2004).
- 40) R. J. Hill, in "The Rietveld Method", Ed. by R. A. Young, Oxford University Press, Oxford (1995) pp. 61–101, p. 95.
- 41) Q. Sun, G. Zeng, J. Li, S. Wang, M. Botifoll, H. Wang, D. Li, F. Ji, J. Cheng, H. Shao, Y. Tian, J. Arbiol, A. Cabot and L. Ci, *Small* **19**, 2302644 (2023).
- 42) X. Gao, S. Li, J. Xue, D. Hu and J. Xu, *Carbon Energy* **5**, 385 (2023).
- 43) X. Gao, W. Lu and J. Xu, *ACS Appl. Mater. Inter.* **13**, 21362 (2021).
- 44) D. Guerard and A. Herold, *Carbon* **13**, 337 (1975).
- 45) N. A. Cañas, P. Einsiedel, O. T. Freitag, C. Heim, M. Steinhauer, D. W. Park and K. A. Friedrich, *Carbon* **116**, 255 (2017).
- 46) W. Bao, C. Fang, D. Cheng, Y. Zhang, B. Lu, D. H. S. Tan, R. Shimizu, B. Sreenarayanan, S. Bai, W. Li, M. Zhang and Y. S. Meng, *Cell Reports Phys. Sci.* **2**, 100597 (2021).
- 47) P.-K. Lee, Y. Li and D. Y. W. Yu, *J. Electrochem. Soc.* **164**, A6206 (2017).
- 48) K. Kitada, O. Pecher, P. C. M. M. Magusin, M. F. Groh, R. S. Weatherup and C. P. Grey, *J. Am. Chem. Soc.* **141**, 7014 (2019).
- 49) K. Pan, F. Zou, M. Canova, Y. Zhu and J. H. Kim, *J. Power Sources* **413**, 20 (2019).